Biosensors and Bioelectronics 124–125 (2019) 1–7

Contents lists available at ScienceDirect

Biosensors and Bioelectronics

journal homepage: www.elsevier.com/locate/bios

A dual signal-on photoelectrochemical immunosensor for sensitively detecting target avian viruses based on AuNPs/g-C_3N_4 coupling with CdTe quantum dots and *in situ* enzymatic generation of electron donor

Bing Sun[a,*], Jing Dong[b], Lin Cui[c], Tiantian Feng[a], Jiujuan Zhu[a], Xuanhe Liu[a], Shiyun Ai[b,*]

[a] School of Science, China University of Geosciences (Beijing), Beijing 100183, China
[b] College of Chemistry and Material Science, Shandong Agricultural University, Taian 271018, China
[c] College of Chemistry, Chemical Engineering and Materials Science, Collaborative Innovation Center of Functionalized Probes for Chemical Imaging in Universities of Shandong, Key Laboratory of Molecular and Nano Probes, Ministry of Education, Shandong Provincial Key Laboratory of Clean Production of Fine Chemicals, Shandong Normal University, Jinan 250014, China

ARTICLE INFO

Keywords:
Photoelectrochemical immunosensor
Signal-on strategy
CdTe quantum dots
Graphitic carbon nitride
Enzymatic catalysis

ABSTRACT

A sensitive and specific photoelectrochemical (PEC) immunosensor was fabricated for subgroup J avian leukosis viruses (ALV-J) analysis based on a dual signal-on strategy. Gold nanoparticles (AuNPs) decorated graphitic carbon nitride (AuNPs/g-C_3N_4) as photoelectrochemical species and primary antibody (Ab_1) against ALV-J were immobilized onto ITO electrode in turn. An ALP-CdTe-Ab_2 bio-conjugant was fabricated by assembling second antibody (Ab_2) and alkaline phosphatase (ALP) to CdTe quantum dots (QDs) surface. The PEC immunosensor was fabricated by successively anchoring the target ALV-J and ALP-CdTe-Ab_2 bio-conjugants onto electrode surface *via* the immune recognition. By virtue of the matched energy levels between CdTe QDs and AuNPs/g-C_3N_4, ALP-CdTe-Ab_2 bio-conjugants could serve as the PEC active probes for photocurrent enhancement. Moreover, the photocurrent response could be further enhanced attributed to the ALP catalytic chemistry to *in situ* produce ascorbic acid for electron donating, achieving an effective dual signal-on mode for PEC assay. On the basis of the ALV-J titers-dependent photocurrent increment, the fabricated PEC immunosensor showed high sensitivity, specificity and stability for ALV-J assay in a wide linear range with a low detection limit of 85 $TCID_{50}$/mL. This PEC immunosensor with the dual signal-on strategy may open up a promising platform for more target analytes in novel immune analysis and clinical diagnostics.

1. Introduction

Exploring and developing an effective and rapid analysis methodology to detect target virus is essential to agriculture, industry as well as human societies. Avian leukosis virus subgroup J (ALV-J) is a class of well-recognized pathogenic species deriving from the recombination of endogenous viral genes to other ALVs (Li et al., 2017b; Venugopal, 1999). Associated with the myeloid leukosis in meat-type chickens, ALV-J infection can suppress the poultry yield, and lead to serious economic losses (Li et al., 2017a; Yun et al., 2013). Developing rapid, low-cost diagnosis and treatment method is effective and convenient to considerably improve the chicken survival rates when ALV-J infection occurs.

Photoelectrochemical (PEC) biosensor is an essential and rapidly developed analysis method based on monitoring the photocurrent or voltage along with the biological interactions between various probing elements and target analysts (Sun and Ai, 2014; Zhao et al., 2015). PEC bioassay features the merits of low-cost, rapid response, high-throughput, simple operation and high sensitivity, and has drawn wide interests in many analysis fields such as enzymatic activity assay (Zhao et al., 2017), pathogenic bacteria detection (Chen et al., 2016; Yang et al., 2018), nucleic acids analysis (Yin et al., 2016; Zhao et al., 2014), cell recognition (Motaghed Mazhabi et al., 2018), and heavy metal ion detection (Li et al., 2018a, 2018b). Benefiting from the advantages of PEC sensors and the inherited high specificity of immunoassay, PEC immunoassay experiences an enormous upswing in the fields of bioassay (Zhao et al., 2018). Two signal-on PEC immunosensors with high sensitivity and specificity in our previous works shed the light on fast detection of ALV-J based on PEC bioassay (Sun et al., 2016, 2014a).

For a robust and versatile PEC immunosensor, the choice of transducer is of vital importance in achieving high sensitivity and excellent analytical performance (Han et al., 2018). As a two-dimensional metal-

* Corresponding authors.
E-mail addresses: sunbing@cugb.edu.cn (B. Sun), ashy@sdau.edu.cn (S. Ai).

https://doi.org/10.1016/j.bios.2018.09.100
Received 26 August 2018; Received in revised form 23 September 2018; Accepted 29 September 2018
Available online 09 October 2018
0956-5663/

free semiconductor with unique electronic features, excellent PEC performance and good stability, graphitic carbon nitride (g-C_3N_4) emerges as an excellent PEC transducer and shows intriguing applications in both biosensor and photocatalysis (Liu et al., 2016; Zhou et al., 2018). In order to overcome the rapid recombination of photogenerated electron-hole pairs and lower carrier conductivity of pure g-C_3N_4, many g-C_3N_4-based nanohybrids have been proposed based on exciton-plasmon reaction (Dong et al., 2017; Li et al., 2017a; Wang et al., 2018; Xu et al., 2017; Zhang et al., 2017b). Quantum dots (QDs) or gold nanoparticles (AuNPs) decorated g-C_3N_4 nanosheets (QDs/g-C_3N_4, AuNPs/g-C_3N_4) are regarded as the great alternatives for fabricating PEC biosensor with excellent analysis performance.

On the other hand, the sensitivity and specificity of PEC immunosensor depend largely on the signal evolution before and after the immune-recognition events (Gong et al., 2016). In order to enhance the photocurrent signal for sensitive PEC immunoassay, some signal-on strategies have been developed based on the catalytic chemistry of enzymes labeled to probing unit (usually be second antibody, Ab_2) (Ren et al., 2017a, 2017b; Sun et al., 2016, 2014a). To some extent, the labeled enzymes could catalyze the substrate molecules to improve the charge transfer in the electrode interfaces, and subsequently enhance the photocurrent response. However, the formed immune-complex on the electrode interface can cause the steric hindrance due to their intrinsic low conductivity, and thus inhibit the diffusion of electron donor or acceptor species to electrode surface for capturing the photogenerated holes or electrons. Lower photocurrent and detection sensitivity are usually obtained. Assembling photoactive species along with the immobilization of probing unit is an effective signal-on strategy to enhance the photocurrent response and improve the detection sensitivity (Shi et al., 2018; Wang et al., 2017a). In this context, versatile QDs (such as CdTe) with tunable particle size and excellent photophysical properties have been used as light-harvesting species in PEC biosensor to sufficiently utilize the light energy and efficiently promote the separation of charge carriers (Shu and Tang, 2017; Wang et al., 2017b). Based on the functionally decorated QDs and the exquisite catalytic chemistry of appropriate enzymes, it is promising to develop a new and more effective dual signal-on strategy for PEC immunosensing.

Herein, we proposed a dual signal-on PEC immunosensor for ALV-J assay by using AuNPs/g-C_3N_4 as photoactive material coupling with mercaptoacetic acid (MPA) capped CdTe QDs integrated with secondary antibody (Ab_2) and alkaline phosphatase (ALP) as both enhanced PEC probes and enzymatic amplification unit. Based on PEC probes immobilization and enzymatically catalytic chemistry for *in situ* generating electron donors, the developed PEC immunosensor revealed the excellent analytic performance for ALV-J detection and could be also extended to other target analytes detection.

2. Experimental sections

2.1. Materials and instruments

Dicyandiamide, tellurium dioxide (TeO_2), $Cd(NO_3)_2$, mercaptoacetic acid (MPA), ascorbic acid (AA), tris(hydroxymethyl)aminomethane (Tris) and chloroauric acid ($HAuCl_4{\cdot}2H_2O$) were purchased from J&K Scientific. Bovine serum albumin (BSA), alkaline phosphatase (ALP), ascorbic acid 2-phosphate trisodium salt (AAP), *N*-(3-dimethylaminopropyl)-*N*-ethylcarbodiimide hydrochloride (EDC) and *N*-hydroxysuccinimide (NHS) were obtained from Sigma-Aldrich (St. Louis, MO). Indium tin oxide (ITO) glass was purchased from Zhuhai Kaivo Electronic Components Co., Ltd. (China, ITO coating 180 ± 25 nm, sheet resistance < 15 Ω/cm^2). All other chemicals were commercially available and used without further purification.

The avian leukosis virus subgroup J and subgroup A (ALV s-J, ALVs-A), ALV-J primary antibody (Ab_1) and second antibody (Ab_2), avian reticuloendotheliosis virus (AREV) were obtained and purified from College of Animal Science and Technology, Shandong Agricultural University (Taian, China). Tris-HCl (10 mM, pH 8.0) buffer solutions were used to prepare PEC detecting buffer (containing 10 mM AAP), blocking buffer (containing 1% w/v BSA), ALP diluting buffer (containing 5 mM $MgCl_2$ and 0.2 mM $ZnCl_2$), and washing buffer (containing 10 mM NaCl). All aqueous solutions were prepared using double distilled water and stored at 4 °C for use. The detecting solutions were deaerated by nitrogen for 15 min before experiments and then kept in a N_2 atmosphere for the entire experimental process.

X-ray diffraction (XRD) experiments were performed on a Bruker D8 Advance diffractometer by using Cu Kα radiation (λ = 1.54056 Å) ranging from 10° to 60° with speed of 3°/min operating at 40 kV voltage and 40 mA current. Transmission electron microscopy (TEM) analysis was conducted with a JEOL JEM-2100 transmission electron microscope at an accelerating voltage of 200 kV. UV–vis absorbance spectra were recorded on a Shimadzu UV 2550 spectrophotometer in the range from 220 to 800 nm. Photoluminescence (PL) spectra were recorded on a Shimazu RF-5301PC spectrophotometer. PEC measurement was performed on a CHI832A electrochemical station (Shanghai Chenhua Apparatus Corporation, China) with a 500 W Xe lamp as the irradiation source (20 mW/cm^2). A typical three electrodes were utilized: the modified ITO electrode (0.20 cm^2) as working electrode, the Pt wire as counter electrode and the saturated calomel electrode (SCE) as reference electrode.

2.2. Preparation of AuNPs modified graphitic carbon nitride (AuNPs/g-C_3N_4)

The g-C_3N_4 was prepared from dicyandiamide through a three-step thermal polymerization. Typically, dicyandiamide (10 g) was loaded in an alumina crucible covered with another one and continuously heated at 220 °C for 2 h, 350 °C for 2 h and 550 °C for 4 h under N_2 atmosphere. The obtained light-yellow products were purified by using deionized water for several times, and finally dried at 60 °C under vacuum condition.

AuNPs/g-C_3N_4 was prepared using the modified method according to previous reports (Chen et al., 2014; Yin et al., 2016). In brief, 60 mg of g-C_3N_4 powders were dispersed in 42 mL of $HAuCl_4$ (0.005, 0.55, 2.75, 5.50 mM, respectively), and stirred in dark for 1 h. Then, 8 mL of methanol was added and the mixture was degassed for 10 min using N_2 and stirred under the ice water bath for 1 h to reduce $HAuCl_4$ and obtain AuNPs. The products were collected by centrifugation at 12,000 rpm and dried under vacuum conditions. The obtained products were denoted as AuNPs/g-C_3N_4-1, AuNPs/g-C_3N_4-2, AuNPs/g-C_3N_4-3, and AuNPs/g-C_3N_4-4, respectively.

2.3. Preparation of MPA-capped CdTe QDs and ALP-CdTe-Ab_2 bio-conjugants

MPA-stabilized CdTe QDs were synthesized by using a slightly modified procedure (Wu et al., 2012; Zhang et al., 2003). Typically, 0.05 g $NaBH_4$ was mixed with 0.01 M TeO_2 in 5 mL N_2-saturated double distilled water to prepare fresh NaHTe solution. $Cd(NO_3)_2$ (1 mM) and MPA (1.8 mM) were dissolved in 50 mL double distilled water. The mixture was degassed under N_2 for 30 min, and adjusted stepwise to pH 11 by using 1 M NaOH. Then the fresh NaHTe was added to the above mixture and refluxed at 100 °C for 2 h to obtain CdTe QDs.

ALP-CdTe-Ab_2 bio-conjugants were prepared using amino linkage. Briefly, 100 μL EDC/NHS mixtures were added to 2 mL MPA-capped CdTe (pH adjusted to 8.0) and shaking for 30 min. Subsequently, Ab_2 (20 μL, 100 U/mL) and ALP (50 μL, 120 U/mL) were added into the solution and reacted for 1 h. The product was centrifuged at 15,000 rpm for 10 min at 4 °C, washed by 10 mM PBS (pH 7.4), centrifuged and finally resuspended in 200 μL of 10 mM PBS (pH 7.4) containing 1% (w/v) BSA, obtaining ALP-CdTe-Ab_2 bio-conjugants.

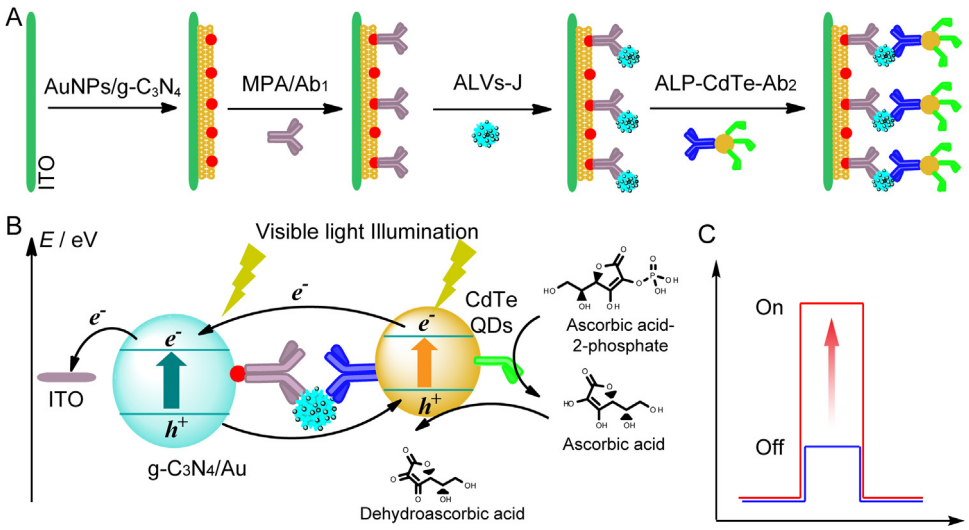

Scheme 1. Schematic illustration for (A) the fabrication of PEC immunosensor and (B) charge carrier transfer route and enzymatic catalysis procedure in PEC detection of ALV-J. (C) Photocurrent turn-on switching in the detection of target avian virus.

2.4. Fabrication of PEC immunosensor for target virus detection

The fabrication procedure of the PEC immunosensor is shown in Scheme 1A. A clean ITO slice with firmed conducting area (0.20 cm^2) was primarily coated by AuNPs/g-C_3N_4 (20 μL, 2 mg/mL suspending in distilled water) and dried under infrared light irradiation to obtain the AuNPs/g-C_3N_4/ITO electrode. After incubated with MPA (20 μL, 5 mM) for 1 h and activated by EDC/NHS for 1 h, Ab_1 (20 μL, 100 U/mL) was added onto the electrode and incubated at 37 °C for 1 h. Then, the modified electrode was washed three times with washing buffer, and the nonspecific binding sites were blocked by 1% BSA for 30 min. The obtained electrode was noted as Ab_1/AuNPs/g-C_3N_4/ITO. Subsequently, the Ab_1/AuNPs/g-C_3N_4/ITO was incubated in 20 μL of ALV-J with different concentrations at 37 °C for 1 h. After incubated with ALP-CdTe-Ab_2 (30 μL) for 1 h and rinsed with electrode washing buffer, the ALP-CdTe-Ab_2/ALV-J/Ab_1/AuNPs/g-C_3N_4/ITO was immersed in the detection buffer (50 mL) under magnetic stirring at 37 °C for 20 min. Finally, the photocurrent response of the modified electrode was recorded in the above solution.

3. Results and discussion

3.1. PEC immunosensor fabrication and sensing principle

As illustrated in Scheme 1A, the PEC immunosensor was fabricated by successively assembling AuNPs/g-C_3N_4 as photoactive layers, primary antibody (Ab_1), target viruses (ALV-J) and ALP-CdTe-Ab_2 bio-conjugants which were prepared by integrating second antibody (Ab_2) and alkaline phosphatase (ALP) to CdTe QDs onto ITO electrode in turn. Based on the immune reaction between Ab and ALV-J, the amount of loaded ALP-CdTe-Ab_2 bio-conjugants increased with raising the concentration of ALV-J. Deriving from the PEC performance and well matched energy levels of AuNPs/g-C_3N_4 and CdTe QDs, ALP-CdTe-Ab_2 bio-conjugants could act as PEC probes to achieve enhanced photocurrent by promoting the ultrafast transfer of photogenerated charge carriers (as highlighted in Scheme 1B). Based on the catalytic effect of ALP in the bio-conjugants, ascorbic acid 2-phosphate (AAP) was enzymatically catalyzed to *in situ* generate ascorbic acid (AA) for efficient electron donating, resulting in the further enhanced photocurrent. The dual signal-on strategy would shed the light on target avian virus analysis with reasonably high sensitivity (Scheme 1C).

3.2. Characterizations of AuNPs/g-C_3N_4

The chemical structure of as-prepared g-C_3N_4 is confirmed by using infrared spectra and X-ray photoelectron spectra as shown in Figs. S1 and S2. The structures of as-prepared AuNPs/g-C_3N_4 are also further investigated by using XRD. As shown in curve a of Fig. 1A, the strong and sharp peak at 27.70° is attributed to characteristic (002) plane diffraction of g-C_3N_4 as a layered graphite-like material. The relatively weak peak at 13.12° can be indexed as (100) plane associated with an in-plane structural packing motif. With the deposition of AuNPs, new diffraction peaks (curves b, c, d, e, Fig. 1A) emerge at 38.27° and 44.43° which are attributed to (111) and (200) planes of AuNPs. No impurity is found. Particularly, the increased intensity of AuNPs diffraction peaks indicates the growing quantity of AuNPs related to the increased concentration of $HAuCl_4$. These results indicate the formation of crystalline g-C_3N_4 and AuNPs/g-C_3N_4.

The morphologies of as-prepared products are illustrated by TEM. Fig. 1B shows that g-C_3N_4 possesses the two-dimensionally extending, almost transparent and sheer-like structures with curled edges. The thinner film obtained may be attributed to the thermal exfoliation in the preparation procedure (Dong et al., 2015). At lower $HAuCl_4$ concentration, the modified AuNPs emerge among g-C_3N_4 nanosheet surface with the average diameter of less than 5 nm (AuNPs/g-C_3N_4-1, Fig. 1C). The AuNPs with increased amounts uniformly distribute on g-C_3N_4 surface in Au/g-C_3N_4-2 (Fig. 1D) and Au/g-C_3N_4-3 (Fig. 1E), and the average particle size increases to *ca.* 8 nm. Particularly, the deposition of AuNPs has no significant impact on the morphology of g-C_3N_4. Further increasing the concentration of $HAuCl_4$ results the formation of aggregated AuNPs with the average size of 35 nm (Au/g-C_3N_4-4, Fig. 1F).

The photophysical properties of AuNPs/g-C_3N_4 are investigated by using UV–vis absorption spectra. As shown in Fig. 2A, both AuNPs/g-C_3N_4 and g-C_3N_4 demonstrate a broad absorption band in the range of visible light. The intrinsic absorption peaks at 235, 340 and 400 nm are attributed to π-π* electron transition in the conjugated aromatic system of g-C_3N_4 (Zhang et al., 2017a). The band gap of pure g-C_3N_4 is evaluated as 2.59 eV (Fig. S3). Comparing to pure g-C_3N_4 (curve a, Fig. 2A), the absorbance of AuNPs/g-C_3N_4 (curves b, c, d, e) is improved along with increasing the amount of AuNPs due to the inherent light absorption and typical surface plasmon resonance absorption of AuNPs. These results imply the formation of AuNPs/g-C_3N_4 hybrids and their enhanced absorption properties.

The photocurrent responses of AuNPs/g-C_3N_4 hybrids are shown in

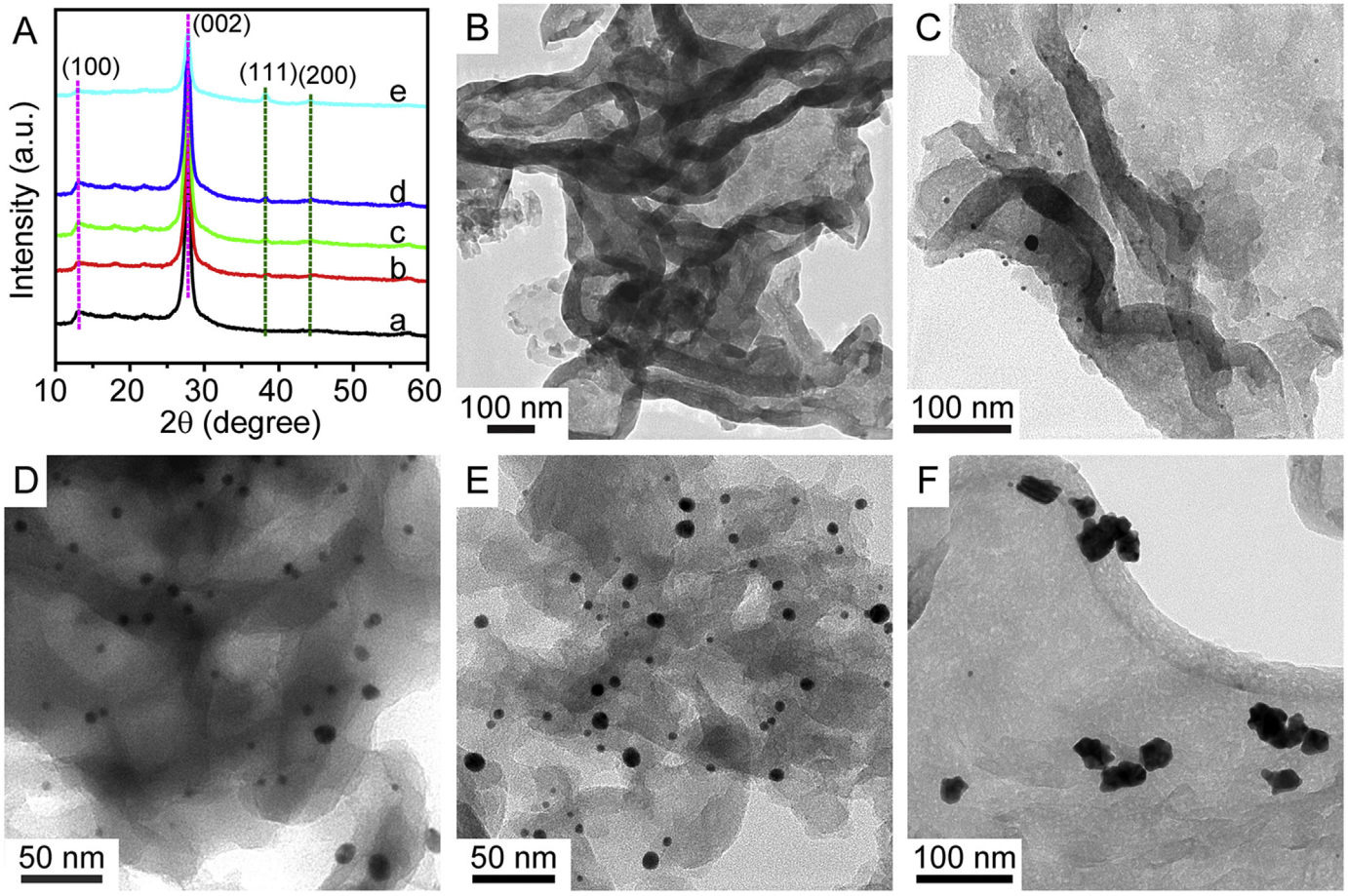

Fig. 1. XRD patterns (A) and TEM images of g-C_3N_4 and AuNPs/g-C_3N_4: (a, B) pure g-C_3N_4, (b, C) AuNPs/g-C_3N_4-1, (c, D) AuNPs/g-C_3N_4-2, (d, E) AuNPs/g-C_3N_4-3, (e, F) AuNPs/g-C_3N_4-4.

Fig. 2B. The photocurrent of pure g-C_3N_4 is *ca.* 500 nA. AuNPs/g-C_3N_4 hybrids show higher photocurrent compared to g-C_3N_4. Particularly, AuNPs/g-C_3N_4-2 possesses the highest photocurrent (up to 693 nA) attributed to the exciton-plasmon reaction (Xu et al., 2017). Further increasing $HAuCl_4$ concentration leads to the decreasing photocurrent, which may be ascribed to the aggregation of AuNPs. The PEC performance is further investigated by using PL spectra. As shown in Fig. 2C, the PL peak at 437.4 nm of pure g-C_3N_4 is significantly quenched with the modification of AuNPs in AuNPs/g-C_3N_4 hybrids. Furthermore, the PL peak is slightly blue shift to 435.9 nm due to the interaction between AuNPs and g-C_3N_4 nanosheets. These results indicate that the deposited AuNPs on the g-C_3N_4 surface can improve the absorption performance to visible light, and can effectively suppress the recombination of photogenerated electron-hole pairs, further leading to the enhanced photocurrent. Under the optimized conditions (2 mg/mL, −0.3 V, Fig. S4), AuNPs/g-C_3N_4-2 is selected as the photoactive layer for fabricating PEC immunosensor.

3.3. Fabrication and characterization of PEC immunosensor

The construction of ALP-CdTe-Ab_2 bio-conjugations is characterized by using UV–vis spectra. As shown in Fig. 3A, the spectra of Ab_2 (curve

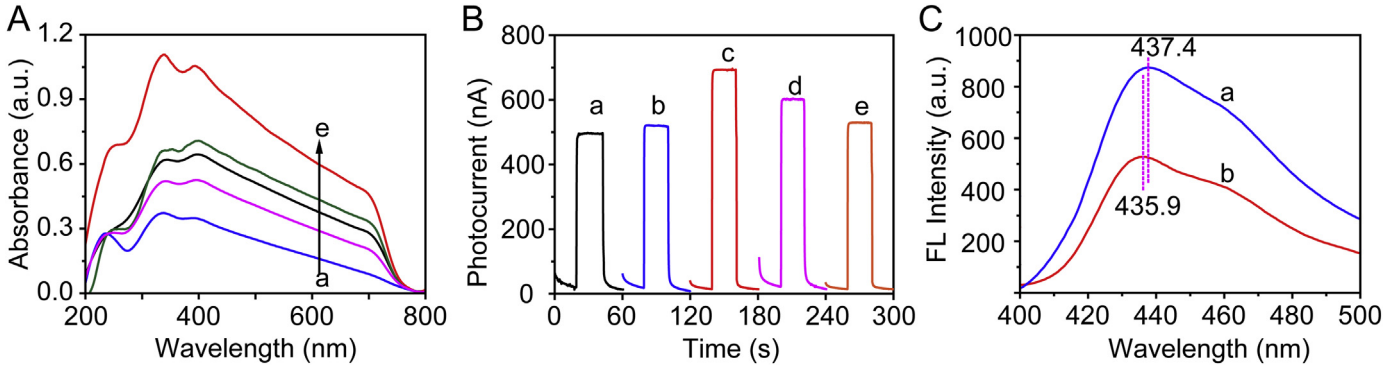

Fig. 2. (A) UV–vis absorption spectra and (B) photocurrent response of different materials under visible light irradiation ($\lambda > 420$ nm) at −0.3 V in PBS (0.01 M pH 8.4) containing AA (0.01 M): (a) g-C_3N_4, (b) AuNPs/g-C_3N_4-1, (c) AuNPs/g-C_3N_4-2, (d) AuNPs/g-C_3N_4-3, (e) AuNPs/g-C_3N_4-4. (C) PL spectra of (a) g-C_3N_4 and (b) AuNPs/g-C_3N_4-2. (λ_{ex} = 338 nm, slit size = 5 nm).

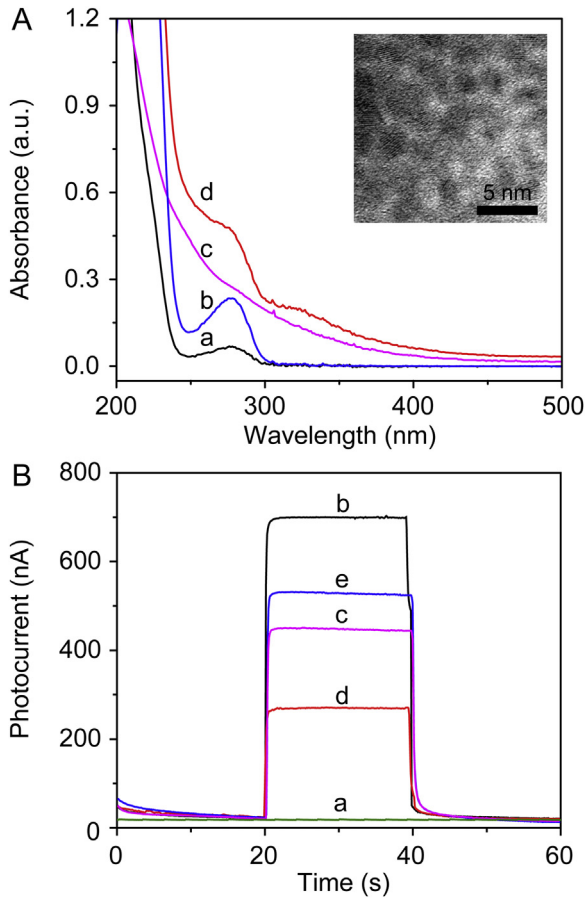

Fig. 3. (A) UV–vis absorption spectra of (a) Ab_2, (b) ALP, (c) CdTe QDs, (d) ALP-CdTe-Ab_2. Insert: High-resolution TEM image of ALP-CdTe-Ab_2. (B) Photocurrent responses of different photoelectrodes in 10 mM Tris-HCl (pH 8.0) containing 10 mM AA: (a) bare ITO, (b) AuNPs/g-C_3N_4-2/ITO, (c) Ab_1/AuNPs/g-C_3N_4-2/ITO, (d) ALV-J/Ab_1/AuNPs/g-C_3N_4-2/ITO, (e) ALP-CdTe-Ab_2/ALV-J/Ab_1/AuNPs/g-C_3N_4-2/ITO.

a) and ALP (curve b) reveal an absorption peak at 276 nm attributed to the absorption of protein in biomaterials. The MAP-capped CdTe QDs exhibit a broad absorption range (curve c). As shown in curve d, the remained absorbance peak at 276 nm and the enhanced absorbance are observed. As shown in high-resolution TEM image inserted in Fig. 3A, the prepared ALP-CdTe-Ab_2 reveals significant lattice fringes with the average size of about 4 nm, indicating the successful preparation of ALP-CdTe-Ab_2 bio-conjugants

The stepwise modification process of the PEC immunosensor is characterized by photocurrent response and EIS as shown in Fig. 3B and Fig. S5. The bare ITO electrode shows a small semi-circle (R_{et}, about 80 Ω, Fig. S5a) implying fast electron transfer, while no significant photocurrent is recorded (curve a, Fig. 3B). When AuNPs/g-C_3N_4-2 is coated to ITO, a remarkable photocurrent is revealed (about 693 nA, curve b, Fig. 3B) although higher R_{et} value is observed (342 Ω, Fig. S5b). After the immobilization of Ab_1 onto electrode surface, increased R_{et} value (466 Ω, Fig. S5c) and decreased photocurrent (440 nA, curve c, Fig. 3B) are recorded for ALV-J/Ab_1/AuNPs/g-C_3N_4-2/ITO photoelectrode. Similar change is also observed for loading ALV-J to Ab_1/AuNPs/g-C_3N_4-2/ITO (photocurrent of 274 nA, curve d, Fig. 3B; R_{et} = 690 Ω, Fig. S5d), which can be assigned to the intrinsic dielectric property of Ab_1 and ALV-J impeding the electron transfer between the donor (AA) and photogenerated holes. Further loading ALP-CdTe-Ab_2 bio-conjugants *via* the specific immunoreaction between ALV-J and Ab_2, the photocurrent significantly increases to 530 nA (curve e, Fig. 3B) although the R_{et} value increases to 862 Ω (Fig. S5e) owing to

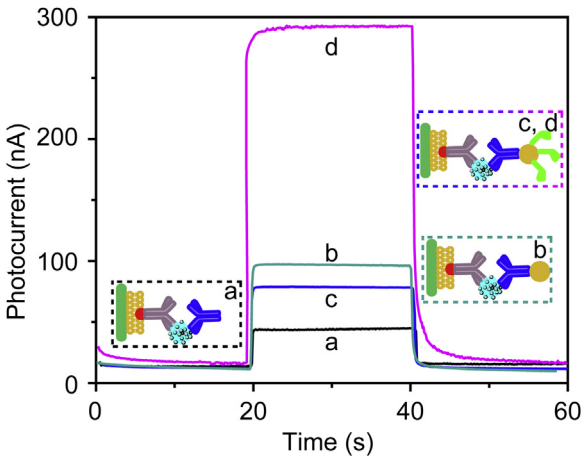

Fig. 4. Photocurrent responses of (a) Ab_2/ALV-J/Ab_1/AuNPs/g-C_3N_4-2/ITO, (b) CdTe-Ab_2/ALV-J/Ab_1/AuNPs/g-C_3N_4-2/ITO and (c) ALP-CdTe-Ab_2/ALV-J/Ab_1/AuNPs/g-C_3N_4-2/ITO photoelectrodes in detecting buffer (ALV-J titer of $10^{3.68}$ $TCID_{50}$/mL). (d) Photocurrent response of ALP-CdTe-Ab_2/ALV-J/Ab_1/AuNPs/g-C_3N_4-2/ITO photoelectrode after enzymatic catalysis by ALP for 20 min in detecting buffer.

the steric hindrance effect. It indicates that the loaded CdTe QDs can further improve the absorption performance of photoelectrode and promote the effective separation of photoinduced electron-hole pairs based on the well matched energy levels between g-C_3N_4 and CdTe QDs, which reliably results in the enhanced photocurrent. These results reasonably demonstrate the successful fabrication of the PEC immunosensor.

3.4. Dual signal-on strategy of the PEC immunosensor

The feasibility of the dual signal-on PEC immunosensor on the basis of the immobilization of PEC probes and *in situ* enzymatically catalyzed electron donor generation is investigated in detecting buffer. As shown in Fig. 4, a weak photocurrent response (*ca.* 43.4 nA) is recorded for only Ab_2 modified ALV-J/Ab_1/AuNPs/g-C_3N_4/ITO photoelectrode (curve a, corresponding to $10^{3.68}$ $TCID_{50}$/mL of ALV-J titer). When CdTe QDs decorated Ab_2 being used, a remarkably increased photocurrent value is obtained (97.2 nA, curve b). Modifying ALP to CdTe QDs attributes to a slightly decreased photocurrent (78.6 nA, curve c). These results are in accordance with that of these photoelectrodes in the presence of AA as electron donor, as shown in Fig. S6. These results indicate that the CdTe QDs loaded along with ALV-J and Ab_2 can act as PEC probes for enhancing the photocurrent response and potential detection sensitivity of the proposed PEC immunosensor.

In order further increasing the photocurrent response and assay sensitivity of PEC immunosensor, a strategy of enzymatically catalytic chemistry is used. As shown in Fig. S7A, the developed ALP-CdTe-Ab_2/ALV-J/Ab_1/AuNPs/g-C_3N_4/ITO electrode shows a low current depending on the swapping potential of cyclic voltammogram in Tris-HCl (10 mM, pH 8.0). And an oxidizing peak around 0.76 V emerges in the presence of AAP. After enzymatic catalysis for a certain time, the CV diagram reveals a redox peak at 0.28 V which can be assigned to the oxidization of generated AA (Sun et al., 2016, 2014b). The enzymatic catalysis time of 20 min is selected based on the enzymatically catalytic time-dependent photocurrent measurements (Fig. S7B). A remarkable photocurrent signal of 293 nA is obtained with the enzymatic catalysis, 3.7 times increased compared to that without enzymatic catalysis (curve d in Fig. 4). As a control experiment by using ALP-Ab_2/ALVs-J/Ab_1/AuNPs/g-C_3N_4-2/ITO photoelectrode (without CdTe QDs), a similar photocurrent signal evolution is recorded before and after enzymatic catalysis (as shown in Fig. S8), while the photocurrent value after enzymatic catalysis is as lower as 86.5 nA. It indicates that the PEC

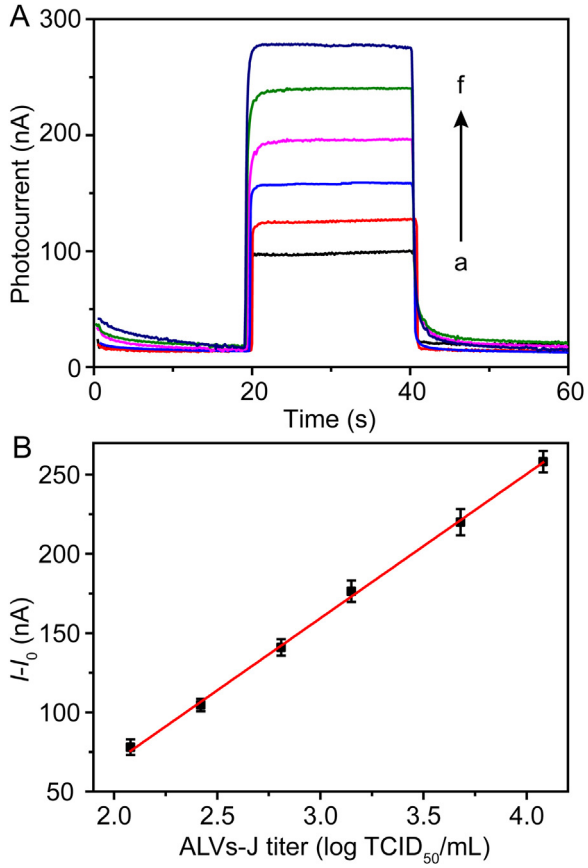

Fig. 5. (A) Photocurrent responses of the PEC immunosensor incubated with various titers of ALV-J and (B) the corresponding calibration plot curve. I and I_0 represent the photocurrent and background current in light-off-state, respectively, in detecting buffer after enzymatic catalysis for 20 min.

probes (CdTe QDs) play an essential role in improving the photocurrent signal of PEC immunosensor. Therefore, ALP-CdTe-Ab_2 bio-conjugants loaded to photoelectrode surface with the concentration of ALV-J can serve as PEC probes for photocurrent enhancement, and also act as enzymatic amplification units to *in situ* generate electron donor for further signal increase. The dual signal-on strategy makes the PEC immunosensor a reliable and feasible platform for ALV-J detection with acceptable sensitivity.

3.5. PEC immunosensing analysis of ALV-J

The PEC immunosensing performance for sensitively quantifying analysis of ALV-J is validated by recording the photocurrent response of PEC immunosensor with varying the ALV-J titer under the optimized conditions. As shown in Fig. 5A, the photocurrent increases gradually with raising the ALV-J titer from $10^{2.08}$ to $10^{4.08}$ $TCID_{50}$/mL. It confirms that the more assembling ALP-CdTe-Ab_2 bioconjugants with raised ALV-J concentration can improve the photocurrent response of PEC electrode by enhancing absorption performance and producing more AA for electron donating. Fig. 5B reveals the linear-dependence of photocurrent to the logarithm of ALV-J titer in the range of $10^{2.08}$–$10^{4.08}$ $TCID_{50}$/mL. The linear equation can be expressed as ΔI (nA) = 91.05 lg c ($TCID_{50}$/mL) – 113.8 (r^2 = 0.9985) with the detection limit of 85 $TCID_{50}$/mL. The acceptable linear range and detection limit are comparable to the previous works (Shang et al., 2013; Sun et al., 2016, 2014b, Supplementary materials Table S1).

3.6. Specificity, reproducibility, and feasibility in real serums

The specificity of the fabricated PEC immunosensor is evaluated against ALVs-A and AREV as the interferents. As shown in Fig. S9A, the photocurrent responses for interferents are lower than that of ALV-J, which are close to that without ALV-J loaded, indicating the good specificity of the PEC immunosensor. The PEC immunosensor also demonstrates an acceptable performance in real sample detection by comparing the photocurrent responses of ALV-J infected serum to the normal serum deriving from chickens. Additionally, the PEC immunosensor reveals good performance against other interferents such as NaCl, vitamin C (VC), BSA and glucose (Fig. S9B). As shown in Fig. S9C, six immunosensors display comparable photocurrent with a relative standard deviation of 6.5%, indicating the acceptable reproducibility of the PEC immunosensor. After storage at 4 °C for a week, 94.6% of the initial photocurrent of freshly fabricated immunosensor remains indicating its good storage stability.

4. Conclusions

In summary, a highly sensitive PEC immunosensor was fabricated for detecting the target avian virus based on the dual signal-on strategy by using ALP-CdTe-Ab_2 bio-conjugants as enhanced PEC probes and enzymatically catalytic elements to *in situ* produce electron donors. AuNPs/g-C_3N_4 hybrids were employed as basic photoactive layers and demonstrated good crystalline structures, improved absorption performance and enhanced photocurrent response. Along with the increased ALV-J titer, more ALP-CdTe-Ab_2 bio-conjugants were immobilized to the modified photoelectrode surface through the immune recognition between antibody and target virus. The PEC immunosensor for ALV-J assay presented a wider linear range with high sensitivity and low detection limit. This strategy may shed light on developing a universal promising platform for novel immune analysis and clinical diagnostics.

Acknowledgements

This work was supported by the Fundamental Research Funds for the Central Universities (No. 2652017143) and the National Natural Science Foundation of China (No. 21802128, 21505086 and 21605096)

Declarations of interest

None.

Appendix A. Supporting information

Supplementary data associated with this article can be found in the online version at doi:10.1016/j.bios.2018.09.100.

References

Chen, H.M., Jheng, K.R., Yu, A.D., 2016. Biosens. Bioelectron. 91, 24–31.
Chen, L., Zeng, X., Si, P., Chen, Y., Chi, Y., Kim, D.H., Chen, G., 2014. Anal. Chem. 86, 4188–4195.
Dong, F., Li, Y., Wang, Z., Ho, W.-K., 2015. Appl. Surf. Sci. 358, 393–403.
Dong, Y.-X., Cao, J.-T., Wang, B., Ma, S.-H., Liu, Y.-M., 2017. ACS Sustain. Chem. Eng. 5, 10840–10848.
Gong, L., Dai, H., Zhang, S., Lin, Y., 2016. Anal. Chem. 88, 5775–5782.
Han, Q., Wang, R., Xing, B., Zhang, T., Khan, M.S., Wu, D., Wei, Q., 2018. Biosens. Bioelectron. 99, 493–499.
Li, H., Li, J., Qiao, Y., Fang, H., Fan, D., Wang, W., 2017a. Sens. Actuators B-Chem. 243, 1027–1033.
Li, H., Li, J., Zhu, Y., Xie, W., Shao, R., Yao, X., Gao, A., Yin, Y., 2018a. Anal. Chem. 90, 5496–5502.
Li, Y., Chen, F., Luan, Z., Zhang, X., 2018b. Biosens. Bioelectron. 119, 63–69.
Li, Y., Cui, S., Li, W., Wang, Y., Cui, Z., Zhao, P., Chang, S., 2017a. BMC Vet. Res. 13, 204.
Li, Y., Fu, J., Cui, S., Meng, F., Cui, Z., Fan, J., Chang, S., Zhao, P., 2017b. Poult. Sci. 96, 1100–1107.
Liu, J., Wang, H., Antonietti, M., 2016. Chem. Soc. Rev. 45, 2308–2326.
Motaghed Mazhabi, R., Ge, L., Jiang, H., Wang, X., 2018. J. Mater. Chem. B 6,

5039–5049.
Ren, X., Ma, H., Zhang, T., Zhang, Y., Yan, T., Du, B., Wei, Q., 2017a. ACS Appl. Mater. Interfaces 9, 37637–37644.
Ren, X., Yan, J., Wu, D., Wei, Q., Wan, Y., 2017b. ACS Sens. 2, 1267–1271.
Shang, K., Wang, X., Sun, B., Cheng, Z., Ai, S., 2013. Biosens. Bioelectron. 45, 40–45.
Shi, X.-M., Mei, L.-P., Wang, Q., Zhao, W.-W., Xu, J.-J., Chen, H.-Y., 2018. Anal. Chem. 90, 4277–4281.
Shu, J., Tang, D., 2017. Chem. Asian J. 12, 2780–2789.
Sun, B., Ai, S.Y., 2014. Prog. Chem. 26, 834–845.
Sun, B., Dong, J., Shi, W.J., Ai, S.Y., 2016. Sens. Actuator B-Chem. 229, 75–81.
Sun, B., Qiao, F., Chen, L., Zhao, Z., Yin, H., Ai, S., 2014a. Biosens. Bioelectron. 54C, 237–243.
Sun, B., Qiao, F.M., Chen, L.J., Zhao, Z., Yin, H.S., Ai, S.Y., 2014b. Biosens. Bioelectron. 54, 237–243.
Venugopal, K., 1999. Res. Vet. Sci. 67, 113–119.
Wang, H., Liu, P., Jiang, W., Li, X., Yin, H., Ai, S., 2017a. Sens. Actuators B-Chem. 244, 458–465.
Wang, X., Xu, R., Sun, X., Wang, Y., Ren, X., Du, B., Wu, D., Wei, Q., 2017b. Biosens. Bioelectron. 96, 239–245.
Wang, Y., Zhou, Y., Xu, L., Han, Z., Yin, H., Ai, S., 2018. Sens. Actuators B-Chem. 257, 237–244.
Wu, S., Dou, J., Zhang, J., Zhang, S., 2012. J. Mater. Chem. 22, 14573–14578.
Xu, L., Ling, S., Li, H., Yan, P., Xia, J., Qiu, J., Wang, K., Li, H., Yuan, S., 2017. Sens. Actuators B-Chem. 240, 308–314.
Yang, Z., Wang, Y., Zhang, D., 2018. Sens. Actuators B-Chem. 274, 228–234.
Yin, H., Zhou, Y., Li, B., Li, X., Yang, Z., Ai, S., Zhang, X., 2016. Sens. Actuators B-Chem. 222, 1119–1126.
Yun, B., Li, D., Zhu, H., Liu, W., Qin, L., Liu, Z., Wu, G., Wang, Y., Qi, X., Gao, H., Wang, X., Gao, Y., 2013. J. Virol. Methods 187, 278–283.
Zhang, G., Savateev, A., Zhao, Y., Li, L., Antonietti, M., 2017a. J. Mater. Chem. A 5, 12723–12728.
Zhang, H., Zhou, Z., Yang, B., Gao, M., 2003. J. Phys. Chem. B 107, 8–13.
Zhang, K., Lv, S., Lin, Z., Tang, D., 2017b. Biosens. Bioelectron. 95, 34–40.
Zhao, W.-W., Xu, J.-J., Chen, H.-Y., 2014. Chem. Rev. 114, 7421–7441.
Zhao, W.-W., Xu, J.-J., Chen, H.-Y., 2015. Chem. Soc. Rev. 44, 729–741.
Zhao, W.-W., Xu, J.-J., Chen, H.-Y., 2017. Biosens. Bioelectron. 92, 294–304.
Zhao, W.-W., Xu, J.-J., Chen, H.-Y., 2018. Anal. Chem. 90, 615–627.
Zhou, Z., Zhang, Y., Shen, Y., Liu, S., Zhang, Y., 2018. Chem. Soc. Rev. 47, 2298–2321.